

Power law viscoelasticity of a fractal colloidal gel

S. Aime,^{1, a)} L. Cipelletti,^{1, b)} and L. Ramos^{1, c)}

Laboratoire Charles Coulomb (L2C),
Univ. Montpellier,
CNRS,
Montpellier,
France

(Dated: 8 October 2018)

Synopsis

Power law rheology is of widespread occurrence in complex materials that are characterized by the presence of a very broad range of microstructural length and time scales. Although phenomenological models able to reproduce the observed rheological features exist, in general a well-established connection with the microscopic origin of this mechanical behavior is still missing. As a model system, this work focuses on a fractal colloidal gel. We thoroughly characterize the linear power law rheology of the sample and its age dependence. We show that at all sample ages and for a variety of rheological tests the gel linear viscoelasticity is very accurately described by a Fractional Maxwell (FM) model, characterized by a power law behavior. Thanks to a unique set-up that couples small-angle static and dynamic light scattering to rheological measurements, we show that in the linear regime shear induces reversible non-affine rearrangements which might be at the origin of the power law rheology and we discuss the possible relationship between the FM model and the microscopic structure of the gel.

PACS numbers: XXX

Keywords: XXX

I. INTRODUCTION

Power law rheology is of widespread occurrence in complex materials that do not exhibit one unique relaxation time, from biomaterials, such as cells Fabry *et al.* (2001); Djordjevic *et al.* (2003); Desprat *et al.* (2005); Balland *et al.* (2006); Kollmannsberger and Fabry (2011); Hecht *et al.* (2015), tissues Kohandel *et al.* (2005); Davis *et al.* (2006); Shen *et al.* (2013), or biopolymer networks Gobeaux *et al.* (2010); Curtis *et al.* (2015) and pastes Józwiak *et al.* (2015), to food science Ma and Barbosa-Cánovas (1996); Zhou and Mulvaney (1998); Subramanian *et al.* (2006); Ng and McKinley (2008); Caggioni *et al.* (2007); Korus *et al.* (2009); Moreira *et al.* (2011); Ronda *et al.* (2013); Xu and Chen (2013); Jaisankar and McKinley (2014); Leocmach *et al.* (2014); Józwiak *et al.* (2015); Faber *et al.* (2017a,b), colloidal gels Rich *et al.* (2011), microgels Lidon *et al.* (2017), hydrogels Hung *et al.* (2015), polymer gels Chambon *et al.* (1986); Winter and Chambon (1986); Durand *et al.* (1987); Martin *et al.* (1988); Adolf and Martin (1990); Tirtaatmadja *et al.* (1997); Larsen and Furst (2008); Leibler *et al.* (1991), melts Plazek (1960); Hernández-Jiménez *et al.* (2002); Friedrich *et al.* (1999), elastomers Curro and Pincus (1983); Winter and Mours (1999); Ferry (1980), and composites Metzler *et al.* (1995). Although the generality of power law rheology is captured by phenomenological models such as the Soft Glassy Rheology model Sollich *et al.* (1997); Sollich (1998), in general a well established connection with the microscopic origin of this mechanical behavior is still missing. Few exceptions include the parallel drawn between power law rheology and microscopic structure and dynamics in the framework of polymer physics. This is for example the case of Rouse motion,

^{a)}Electronic mail: stefano.aime@gmail.com.

^{b)}Electronic mail: Luca.Cipelletti@umontpellier.fr.

^{c)}Electronic mail: Laurence.Ramos@umontpellier.fr.

where the self-similar relaxation dynamics naturally come into play as a consequence of the fractal nature of the polymer coil Colby and Rubinstein (2003). In this case, the fractal dimension $d_f = 2$ describing the microscopic structure is directly linked to the fractional order of the rheological model, i.e. the exponent $\alpha = 0.5$ describing the power law rheology. Similarly, in the attempt of modeling polymer gels at the critical point, Adolf and Martin Adolf and Martin (1990) explicitly derive a power law distribution of relaxation times from a postulated scale-independence, which is assumed to hold at the critical gel point according to percolation theory Stauffer and Aharony (2003), in quantitative agreement with a direct measurement of the fractal mass distribution Martin and Adolf (1991). More generally, a quantitative link between power law rheology and the microscopic structures of critical gels with arbitrary fractal dimension is established by Muthukumar Muthukumar (1989) in the two limit cases of screened and unscreened excluded volume and hydrodynamic interactions. This model essentially extends Rouse dynamics from a single chain to a branched, fractal object. In this case the mathematical formulation is much more involved, but, as in Rouse dynamics, the power law rheology reveals the self-similarity of microscopic dynamics, stemming from the fractal structure Patrício *et al.* (2015). Accordingly, the direct link between fractal structure and power law rheology has proved to properly describe several experimental results on various polymer networks Dahesh *et al.* (2016); Takenaka *et al.* (2004); Matsumoto *et al.* (1992). Although fractal structures are very well represented in soft materials, from human tissues Helmberger *et al.* (2014); Mauroy *et al.* (2004); Ahmadi *et al.* (2013) to polymer and colloidal gels Martin and Adolf (1991); Carpineti and Giglio (1993); Bremer *et al.* (1990), the wide spectrum of systems displaying a power law rheology suggests that power law rheology does not necessarily stem from fractal structure, and that other microscopic mechanisms might produce power law distributions of relaxation times as well. In the absence of a full understanding of such mechanisms, however, fractional rheological models that consider fractional derivatives of the stress and/or the strain in the constitutive equations remain largely phenomenological, and the amount of relevant physical information that can be extracted from them remains arguable.

In this regard, one crucial aspect is the scarcity of systems for which a thorough discussion of linear rheology is available. Indeed, the majority of the works finding a power law rheology only focuses on oscillatory shear Ma and Barbosa-Cánovas (1996); Metzler *et al.* (1995); Tirtaatmadja *et al.* (1997); Fabry *et al.* (2001); Djordjevic *et al.* (2003); Shen *et al.* (2013); Caggioni *et al.* (2007); Rich *et al.* (2011); Hung *et al.* (2015); Friedrich *et al.* (1999), whereas others only focus on transient experiments, either stress relaxation Hernández-Jiménez *et al.* (2002); Curro and Pincus (1983), creep Desprat *et al.* (2005); Xu and Chen (2013) or both Davis *et al.* (2006). Transient experiments alone are delicate, and have to be carefully performed in order to ensure that only the linear regime is being probed, since sometimes power law creep clearly emerges as a nonlinear phenomenon Duval *et al.* (2010); Paredes *et al.* (2013). Indeed, plastic power law creep is observed for many systems, from crystalline materials like metals Andrade (1910); Miguel *et al.* (2002); Poirier (1985); Cottrell (1952) or ice Ashby and Duval (1985) to colloidal Siebenbürger *et al.* (2012); Sentjabrskaja *et al.* (2015); Coussot *et al.* (2006); Caton and Baravian (2008) or polymeric Nechad *et al.* (2005); Karobi *et al.* (2016) systems, which would have a very different rheology in the linear regime. On the other hand, the challenge of oscillatory shear is that it typically gives access to a limited range of frequencies, which sometimes makes it difficult to distinguish the predictions of different models. Moreover, measurements are even more difficult for non-stationary, aging, systems, although clever techniques exist to overcome those limitations Ghiringhelli *et al.* (2012); Bouzid *et al.* (2018); Geri *et al.* (2018). In some systems a larger spectrum can be accessed exploiting time temperature superposition, although its applicability is far from being trivial in most systems cited above.

One instructive example in this regard is represented by various independent works on flour doughs Korus *et al.* (2009); Moreira *et al.* (2011); Ronda *et al.* (2013), where oscillatory rheology revealed clear power law responses, whereas creep and recovery on the same samples were nicely fitted by a Burger model, which predicts an exponential creep. In another example on polymer microgels, a power law rheology was found in both oscil-

latory shear and creep, but described by incompatible power law exponents Lidon *et al.* (2017), which also questions the applicability of a fractional model. Moreover, for polymer melts, a power law creep was also interpreted as the short time limit of a stretched exponential Cherière *et al.* (1997). All these examples show that a comparison between different rheological measurements is essential to truly validate a phenomenological model. This is done for example on individual cells Balland *et al.* (2006), but also on collagen networks Gobeaux *et al.* (2010), biopolymer gels Ng and McKinley (2008); Leocmach *et al.* (2014), natural gums Jaishankar and McKinley (2014) and cheese Faber *et al.* (2017b). For these systems, fractional rheological models provide a consistent description of the observed rheology. However, most of these systems are rather complex, and their structural analysis is delicate, rendering virtually difficult clear connections between rheological and structural properties.

In this paper we focus on a simpler model system, namely a colloidal gel, for which both microscopic structure and spontaneous dynamics are well known and can be easily measured with scattering methods Carpineti *et al.* (1995); Cipelletti *et al.* (2000). Thanks to a careful analysis of both oscillatory and transient shear we show that the linear rheology is consistently described by a Fractional Maxwell model, whose parameters are discussed in detail, with reference to the sample structure and to its aging properties. By coupling rheology to light scattering, we moreover demonstrate that, in the linear viscoelastic regime, the shear deformation provokes microscopic rearrangements that are fully reversible. The paper is organized as follows: after reviewing the theoretical background (Sec. II), we describe the sample preparation and the experimental setup (Sec. III). In Sec. IV the rheological results are shown and fully described with the linear viscoelastic model, and the link to structural data is established thanks to a set-up that couples small-angle light scattering to rheological measurements. A conclusive section (Sec. V) closes the manuscript, with a detailed discussion about the link between the rheological properties and the microscopic structure.

II. THEORETICAL BACKGROUND

We recall here the theoretical basis for fractional rheology, which can be found in greater detail in Refs. R. Hilfer (2000); Jaishankar and McKinley (2013)

A. Fractional derivatives in rheology

For systems characterized by a power law rheology, the relaxation modulus measured, e.g., in a step strain experiment, decays as $G(t) \propto t^{-\alpha}$ with $0 < \alpha < 1$. For such systems, fractional expressions come naturally into play as a result of the superposition principle. Indeed, the stress response to an arbitrary shear history $\gamma(t)$ is given by the convolution integral R. Hilfer (2000):

$$\sigma(t) = \frac{K}{\Gamma(1-\alpha)} \tau^\alpha \int_{-\infty}^t (t-t')^{-\alpha} \dot{\gamma}(t') dt' \quad (1)$$

Here K is a modulus and τ is a characteristic time. In this expression one recognizes the fractional derivative of order α , d^α/dt^α , which is defined as $\Gamma(1-\alpha) d^\alpha \gamma / dt^\alpha = \int_{-\infty}^t (t-t')^{-\alpha} \dot{\gamma}(t') dt'$ Demirci and Ozalp (2012). Hence,

$$\sigma(t) = K \tau^\alpha \frac{d^\alpha \gamma}{dt^\alpha} \quad (2)$$

By inverting the above equation, one finds for example that the creep deformation of the material in response to a step stress applied at time $t = 0$, $\sigma(t) = \sigma_0 \Theta(t)$, with $\Theta(t)$ the Heaviside step function, is a power law:

$$\gamma(t) = K^{-1} \tau^{-\alpha} \frac{d^{-\alpha}}{dt^{-\alpha}} \sigma(t) = \frac{\sigma_0}{K} \frac{\Theta(t)}{\Gamma(1+\alpha)} \left(\frac{t}{\tau}\right)^\alpha \quad (3)$$

For $\alpha = 1$ one recovers the linear flow of a dashpot element, $\gamma(t) = \sigma_0 t / K\tau$ (for $t \geq 0$), where $K\tau$ is a viscosity. On the other hand, for $\alpha = 0$, one recovers the step strain of an elastic spring of elastic modulus K , $\gamma(t) = \sigma_0 / K$. In the general case ($0 < \alpha < 1$), Eq. 3 corresponds to a fractional rheological element called Scott-Blair element or springpot Blair *et al.* (1947); Bagley and Torvik (1983, 1986). Figure 1 (top) reproduces the creep profiles expected for springpot elements with different values of the fractional exponent α and shows a smooth and continuous transition from a viscous liquid to an elastic solid.

B. Fractional Maxwell Model

The Fractional Maxwell (FM) model is based on two springpots in series, and is thus characterized by four independent parameters, which can be interpreted as an elastic modulus G_0 , a characteristic time τ_{FM} , and two exponents α and β . In the following, we will consider the special case where one of the two springpots is reduced to an elastic spring ($\beta = 0$). In this case the rheological constitutive equation reads:

$$\frac{d^\alpha \gamma}{dt^\alpha} = \frac{1}{G_0} \left[\frac{\sigma(t)}{\tau_{FM}^\alpha} + \frac{d^\alpha \sigma}{dt^\alpha} \right] \quad (4)$$

Note that, for $\alpha = 1$, Eq. 4 corresponds to a standard Maxwell fluid.

Solutions of the FM model for standard rheological experiments have been previously computed Bagley (1989); Jaishankar and McKinley (2013, 2014); Józwiak *et al.* (2015). For a sinusoidal deformation of angular frequency ω , the storage, G' , and loss, G'' , moduli read:

$$G'(\omega) = G_0 \zeta \frac{\cos(\frac{\pi}{2}\alpha) + \zeta}{1 + \zeta^2 + 2\zeta \cos(\frac{\pi}{2}\alpha)} \quad (5)$$

$$G''(\omega) = G_0 \zeta \frac{\sin(\frac{\pi}{2}\alpha)}{1 + \zeta^2 + 2\zeta \cos(\frac{\pi}{2}\alpha)} \quad (6)$$

where $\zeta = (\omega \tau_{FM})^\alpha$.

On the other hand, the creep deformation following the application at time $t = 0$ of a step stress of amplitude σ_0 reads:

$$\gamma(t) = \frac{\sigma_0}{G_0} \left[1 + \frac{1}{\Gamma(\alpha+1)} \left(\frac{t}{\tau_{FM}}\right)^\alpha \right] \quad (7)$$

This equation can be decomposed as follows:

$$\gamma(t) = \gamma_e^+ + \gamma_{\text{creep}}(t) \quad (8)$$

Here $\gamma_e^+ = \sigma_0 / G_0$ is the instantaneous elastic part of the mechanical response and $\gamma_{\text{creep}}(t) = \frac{\gamma_e}{\Gamma(\alpha+1)} \left(\frac{t}{\tau_{FM}}\right)^\alpha$ is analogous to Eq. 3 and corresponds to the cumulated creep deformation since the application of the step stress at time $t = 0$.

It is also interesting to investigate the creep recovery, that is the time evolution of the deformation following the release of the stress σ_0 at time T . We here define $t' = t - T$ as the time elapsed since the release of the stress, which has been applied from time $t = 0$ to time T . Similarly to the creep, the creep recovery is composed of an instantaneous elastic relaxation of amplitude $\gamma_e^- = \sigma_0/G_0$ and a slow decay function $\gamma_{\text{rec}}(t')$ that reads:

$$\gamma_{\text{rec}}(t') = \gamma_{\text{creep}}(T) \left[\left(1 + \frac{t'}{T}\right)^\alpha - \left(\frac{t'}{T}\right)^\alpha \right] \quad (9)$$

We observe that the linear viscoelastic creep of a FM model is completely reversible, since $\gamma_{\text{rec}}(t' \rightarrow \infty) = 0$. Interestingly, Eq. 9 predicts that the initial un-deformed configuration is recovered with a characteristic time that uniquely depends on the duration T of the creep, whereas it is independent of the natural timescale τ_{FM} . We show in Fig. 1b the creep and recovery for a Fractional Maxwell model with a representative value of $\alpha = 0.5$ together with the asymptotic behaviors, a Maxwell fluid ($\alpha = 1$) and an elastic solid ($\alpha = 0$).

III. MATERIAL AND METHODS

A. Sample

We investigate a fractal colloidal gel. The gel is formed by aggregating a water suspension of charged silica particles (Ludox TM50, from Sigma Aldrich) (of diameter 25 nm) at a volume fraction $\phi = 5\%$. Particle aggregation is triggered by increasing *in situ* the ionic strength of the solvent, thanks to the hydrolysis of urea into carbon dioxide and ammonia: $\text{CO}(\text{NH}_2)_2 + \text{H}_2\text{O} \rightarrow \text{CO}_2 + 2\text{NH}_3 \rightarrow \text{NH}_4^+ + \text{NH}_3 + \text{HCO}_3^-$. This chemical reaction is catalyzed by an enzyme (Urease U1500-20KU, from Sigma Aldrich), which increases the ionic strength of the solvent and thus screens the electrostatic repulsion between particles, eventually inducing particle aggregation Wyss *et al.* (2004). Adding urea (concentration 1 Mol/l) and urease (35 U/ml) to the colloidal suspension at room temperature induces a sol-gel transition of the suspension within roughly 3 hours. Structural information on the gel and on the particles are obtained by neutron and light scattering techniques. In order to increase the contrast between the particles and the solvent in neutron scattering, water (H_2O) is replaced by heavy water (D_2O), without any indication of any structural and rheological alteration of the sample following the replacement of H_2O by D_2O .

B. Scattering techniques and rheology

The structure of the sample is probed combining different scattering techniques, allowing one to access a wide range of scattering vectors q , from 0.1 to 2000 μm^{-1} . We use small-angle neutron scattering (SANS) (PA20 beamline at Laboratoire Léon Brillouin, France), and custom made wide-angle (WALS) and small-angle light scattering setups (SALS) Tamborini and Cipelletti (2012). For SANS, the sample is held in a 2 mm thick rectangular cell, whereas for light scattering experiments the cell thickness was decreased to 1 mm in order to avoid multiple scattering.

Rheological measurements are performed in the Couette cell of a stress-controlled rheometer (Anton Paar MCR502), with a low viscosity silicon oil film on top of the sample to prevent evaporation over very long timescales (several weeks). Frequency sweep, respectively creep, measurements are performed at sufficiently small strain amplitude (typically $\gamma_0 = 0.1\%$), resp. at sufficiently small applied stress, to ensure data are acquired in the linear regime. Strain sweep experiments are also conducted at 1 Hz to determine the upper bound of the linear regime. For the frequency sweep during sample aging, we choose a protocol that minimizes the impact of the finite experimental time on the measured viscoelastic moduli: we perform high-to-low and low-to-high frequency sweeps one after the other, and

for each frequency we take the average of the moduli measured during the two sweeps. The waiting time t_w reported in each plot corresponds to the average between the times of the two measurements, and is the same for all frequencies. Except at very short aging time, the duration of one frequency sweep is short compared to the sample aging time, hence ensuring reliable results.

In addition, the sample structure, dynamics and rheological properties are also probed simultaneously using a custom made SALS apparatus Tamborini and Cipelletti (2012), which is coupled to a linear, parallel plate stress-controlled shear cell Aime *et al.* (2016). The setup allows one to access scattering vectors q ranging from about $0.2 \mu\text{m}^{-1}$ to $4 \mu\text{m}^{-1}$, essentially oriented in the (vorticity, velocity) plane, with a minor q -dependent component along the shear gradient direction. Static and dynamic light scattering experiments under oscillatory shear are performed as described in Aime *et al.* (2018). In static light scattering experiments one measures the time-averaged intensity scattered as a function of the scattering vector q , from which information on the particle size and interparticle correlations can be extracted Zemb and Lindner (2002). On the other hand, in dynamic experiments one measures the two-time intensity correlation function $g_2(\vec{q}, t_1, t_2) - 1 \propto |g_1(\vec{q}, t_1, t_2)|^2$, where g_1 is the intermediate scattering function, quantifying the relative displacements of the scatterers along the scattering vector \vec{q} Berne and Pecora (2013). Under shear, the field describing particle displacements is generally anisotropic, and can be decoupled into an affine contribution, always in the shear direction \hat{e}_{\parallel} , and a nonaffine contribution, which typically has nonzero components perpendicular to \hat{e}_{\parallel} . In the scattering geometry, it is thus possible to decouple the two contributions by looking at scattering vectors oriented in the vorticity direction (\vec{q}_{\perp}), which only carry information about nonaffine rearrangements whereas scattering vectors oriented in the velocity direction (\vec{q}_{\parallel}) contain contributions from both affine and non-affine displacements.

All experiments are performed at room temperature. For both scattering measurements and rheological measurements, the sample is loaded in the scattering or shear cell while still in a liquid state and is then allowed to gel *in-situ*. By monitoring the sample at rest over long time, we observe that the gel is stable, and we can neglect the influence of gravity on the microscopic structure.

IV. RESULTS

A. Sample structure

We show in Fig. 2 the scattering profiles, i.e. the scattered intensity, I , normalized by particle volume fraction, ϕ , of a dilute, liquid and stable suspension ($\phi = 0.037 \%$) and of a colloidal gel ($\phi = 5 \%$) as a function of the scattering vector q , over several orders of magnitude, thanks to the combination of three experimental techniques (SANS, WALS and SALS). Over the whole range of scattering vectors investigated, the scattering profile of the dilute suspension can be quantitatively accounted for by the form factor of polydisperse spherical particles Bressler *et al.* (2015): $I(q) = \int \rho(R)P(q, R)dR$, where $P(q, R) = \left[3(\sin(qR) - qR \cos(qR))(qR)^{-3}\right]^2$ is the form factor of a uniform sphere of radius R , and the weighting function $\rho(R)$ is derived from a Gaussian distribution of particle sizes. The best fit of the experimental data (continuous line in Fig. 2) yields an average diameter $a = 25 \text{ nm}$ and a 10 % polydispersity (defined as the full width at half maximum of the particle size distribution). For the colloidal gel, one sees that the data at large q , which probe the structure of the individual particles, perfectly superimpose with the measurement for the dilute suspension, as expected. By contrast, data for $q < 200 \mu\text{m}^{-1}$ largely differ. The scattered intensity is the one expected for crowded fractal clusters of particles Carpineti and Giglio (1993); Manley *et al.* (2005a). For q in the range $(10 - 200) \mu\text{m}^{-1}$, I decays as q^{-2} , indicating a fractal dimension $d_f = 2$. At very low q ($q < q^*$, with $q^* \approx 10 \mu\text{m}^{-1}$), the scattered intensity becomes almost q -independent, indicating that on length scales larger

than $2\pi/q^* \approx 0.6 \mu\text{m}$, the sample structure is rather homogeneous. This value is in good numerical agreement with the theoretical expectation for the cluster size $\xi \sim a\phi^{1/(d_f-3)} \sim 1 \mu\text{m}$ Carpineti and Giglio (1992).

B. Gelation dynamics

Gelation dynamics is probed by dynamic light scattering. At early stages, right after preparation, the sample is a liquid with a viscosity comparable to that of water. As a consequence of enzymatic activity, the ionic strength of the solvent grows in time, and after an induction time that depends on the amount of enzyme added (typically 8000 s in our experiments), it becomes large enough to trigger particle aggregation. This event can be clearly seen with dynamic light scattering, since the formation of larger particle clusters slows down the microscopic dynamics. A few minutes after the onset of aggregation, the relaxation time τ_R becomes measurable for most accessed scattering vectors. The scaling $\tau_R \sim q^{-2}$ confirms that we probe the diffusive motion of the aggregates. With time, the decay of the correlation functions shifts towards larger delays, showing that the aggregates are growing in size. Eventually, clusters become large enough to touch each other, and at that moment a system-spanning network is formed. When this happens, the dynamics slows down tremendously and changes qualitatively, with correlation functions changing from simple exponentials to compressed exponentials and the τ_R scaling changing from q^{-2} (diffusive-like dynamics) to q^{-1} (ballistic-like dynamics) (Fig. 3c), as observed for many soft solid materials Cipelletti *et al.* (2000); Cipelletti and Ramos (2005).

C. Linear viscoelasticity

1. Frequency sweep during aging

As a network forms, a finite storage modulus G' is measured by rheometry. Subsequently, the rheological response of the material rapidly evolves with time towards the elasticity-dominated pattern shown in Fig. 4a. One defines the sample age t_w as the time elapsed since the gelation time, chosen at the time of crossover between G' and G'' , as measured at an angular frequency $\omega = 0.628 \text{ rad/s}$.

We probe the evolution with sample age of the frequency dependence of the complex modulus. Data are measured for t_w spanning more than 3 orders of magnitude (from 300 s to 8×10^5 s). Over this timescale, the storage modulus increases by almost 3 orders of magnitude, and the loss modulus by more than 2 orders of magnitude. Interestingly, all along the aging process, the sample viscoelasticity is always very well described by the Fractional Maxwell model Jaishankar and McKinley (2013), as shown in Fig. 4a where the best fits of the experimental data using Eqs. 5 and 6 are displayed.

The evolution of the fit parameters α , τ_{FM} and G_0 upon sample aging are given in Fig. 5. Although the data are somehow noisy, the exponent α is measured to slightly decrease with sample age, from ~ 0.42 to ~ 0.32 , in analogy to what found in the literature on biopolymer gels Curtis *et al.* (2015). On the other hand, the elastic modulus, G_0 , and the characteristic time, τ_{FM} , display a smooth and continuous increase with t_w . Both parameters are measured to increase rather rapidly at short time ($t_w \lesssim 10^4$ s), and less steeply at longer times. In the late time regime, we find $\tau_{\text{FM}} \sim t_w$, with τ_{FM} about one order of magnitude smaller than the waiting time and $G_0 \sim t_w^{1/3}$. Note that the scaling law measured for the elastic modulus with sample age is similar to previous findings for other colloidal gels Manley *et al.* (2005b); Koumakis and Petekidis (2011); Guo *et al.* (2011); Calzolari *et al.* (2017).

2. Creep experiments for old samples

To check for consistency as well as to probe smaller frequencies, we perform creep experiments in the linear regime. Typical creep profiles are shown in Fig. 4b for different waiting times t_w , in the range $(1.2 - 5.4) \cdot 10^5$ s. Here the sample is rather old, ensuring that during each creep measurement, which lasts 10000 s at most, sample aging is negligible. The shear stress is fixed at $\sigma_0 = 30$ Pa and is about 2 orders of magnitude smaller than the elastic modulus, such that measurements are performed in the linear regime. Indeed, a strain sweep on an old sample ($t_w = 24 \times 10^5$ s) shows that linearity extends beyond 1% deformation (Fig. 6).

As the sample ages and G_0 increases, the initial elastic jump for a fixed applied stress becomes smaller, and the further increase with time of the strain becomes smaller as well. For all sample ages investigated (between 10^5 and 10^6 s), we find that the whole time evolution of the strain is very well fitted by the theoretical prediction of the FM model (Eq. 7), with parameter values that are fully consistent with those measured in oscillatory experiments (see squares in Fig. 5). To further prove the appropriateness of the FM model, we plot the data in rescaled units, $\tilde{X} = \frac{1}{\Gamma(\alpha+1)} \left(\frac{t}{\tau_{FM}} \right)^\alpha$ and $\tilde{Y} = \frac{G_0 \gamma}{\sigma} - 1$. We find a nice collapse onto a single curve, which is moreover in perfect agreement with the theoretical expectation $\tilde{Y} = \tilde{X}$ (Eq. 7).

A direct comparison of creep and frequency sweep measurements can be achieved using methods available in literature Evans *et al.* (2009). As an illustration, we show in Fig. 7 the direct measurement of the frequency-dependence of the storage and loss moduli, together with the frequency dependence of G' and G'' computed from a creep experiment Evans *et al.* (2009), and the fit using the FM model. We find a nice overlap of the two sets of data. Importantly, creep measurements allow the measurements to be extended at lower frequency as compared to oscillatory rheology, about one decade for the data shown in Fig. 7. These data allow one to probe the sample behavior almost up to the FM characteristic time τ_{FM} . At low angular frequencies ($\omega \ll \tau_{FM}^{-1}$), both G' and G'' increase as ω^α , whereas in the high angular frequency regime ($\omega \gg \tau_{FM}^{-1}$), $G' \sim G_0$ and $G'' \propto \omega^{-\alpha}$.

Overall, we find that the evolution of the three parameters of the FM model as extracted from oscillatory shear and creep experiments nicely overlap over the whole range of sample ages. This demonstrates the relevance of the Fractional Maxwell model to describe the linear viscoelasticity of our fractal colloidal gel.

3. Creep-recovery experiments

To further test the FM model, we perform creep recovery experiments. Here, after a creep of duration T , the stress is released, and the sample is left at rest until the creep strain is fully relaxed, before applying another step stress. T is chosen such that the sample age ($t_w > 10^5$ s) is much larger than the duration of the experiment, in order to keep aging effects negligible during creep. The strain evolution during a representative creep and recovery experiment is shown in Fig. 8a, together with the fit with the FM model (Eq. 8 for the creep and Eq. 9 for the recovery). We find that the FM reproduces extremely well the experimental data. Interestingly, we measure that, for initial elastic jumps γ_e^+ up to 3.5% (obtained by imposing various stress amplitudes), the instantaneous recovery γ_e^- is exactly equal to γ_e^+ (inset Fig. 8). Such equality provides a further indication that the experimental data correspond to the linear viscoelastic regime, in agreement with the findings for the oscillatory and creep experiments.

Typical strain relaxations during creep recovery are shown in Fig. 8b for an old sample ($t_w \approx 5 \cdot 10^5$ s) that has been submitted to three consecutive creep tests of duration $T = 100, 1000$ and 10000 s. We find that as the duration of the creep is longer, the initial value of γ in the creep recovery is higher, as expected. Equation 9 predicts that after the sudden release of the external stress the macroscopic deformation should decay to 0 with a characteristic

shape depending on α and scaling as t'/T . Figure 8d shows that the t'/T scaling does indeed hold, since data measured for different creep durations collapse on a single curve once the strain is normalized by the strain cumulated at the end of the previous creep step ($\gamma_{\text{creep}}(T)$, cf. Eq. 8), and time t' is normalized by the creep duration T .

The data shown in Fig. 8 show that creep recovery experiments are also in good quantitative agreement with FM predictions, and that the cumulated strain γ almost fully relaxes to 0. This suggests that the rearrangements occurring during creep are reversible, despite the sample is not purely elastic.

D. Reversibility

1. Structural anisotropy

We check for reversibility at a microscopic level by direct structural measurements during a sinusoidal shear deformation, using the home-made set-up that couples small-angle light scattering to a stress-controlled shear cell described in Aime *et al.* (2016). The microscopic structure of the sample is monitored as a function of time during sample deformation for rheological tests similar to those performed in a classical rheometer and presented above. Over the range of wave-vectors q probed (between 0.4 and 4 μm^{-1}), the scattered intensity does not evolve, suggesting that the structure of the colloidal gel is fundamentally preserved under deformation in the linear regime. However, as the sample is sheared, a small anisotropy (a few percents) in the static structure factor is detected. Such anisotropy has already been observed in simulations Park *et al.* (2017); Colombo and Del Gado (2014); Bouzid and Del Gado (2018); Jamali *et al.* (2017) and measured in experimental works on colloidal gels Mohraz and Solomon (2005); Vermant and Solomon (2005); Kim *et al.* (2014). It has been interpreted as the signature of structural alignment in the direction of flow.

In particular, in our experiments we find that the intensity of the light scattered in the direction perpendicular to the shear direction (vorticity direction), $I(\vec{q}_\perp)$, is constant, whereas the one scattered in the parallel (velocity) direction, $I(\vec{q}_\parallel)$, changes roughly linearly with the macroscopic deformation. To quantify this effect, we define a static anisotropy parameter $\chi(q) = [I(\vec{q}_\parallel) - I(\vec{q}_\perp)] / [I(\vec{q}_\parallel) + I(\vec{q}_\perp)]$. We find that the anisotropy $\chi(q)$ nicely follows the evolution of the strain when the sample is submitted to a small oscillatory stress, as illustrated in Fig. 9a for $\sigma_0/G_0 = 4\%$ and $q = 2.6 \mu\text{m}^{-1}$. Similarly, χ roughly follows the time evolution of the measured macroscopic strain during a creep and creep recovery experiment (Fig. 9c). Overall, our data show that, in the linear regime, the structural anisotropy is proportional to the strain applied and is therefore fully reversible. More quantitatively, we plot χ as a function of the strain amplitude γ_e in Fig. 9b. For $-4\% < \gamma_e < +4\%$, we can empirically model the observed asymmetry with the linear relation $\chi(q, \gamma) = k(q)\gamma$, with the factor $k(q)$ a phenomenological proportionality constant that increases roughly linearly with q (inset of Fig. 9b). Consistently, 4% correspond to the limit of the linear regime as defined from the maximum strain amplitude at which the complex moduli are independent of the strain amplitude (Fig. 6). Beyond $\gamma = 4\%$, an excess of anisotropy is measured, corresponding to the onset of rheological non-linearity.

2. Non-affine dynamics and microscopic reversibility

The reversibility of the imposed deformation is confirmed at a microscopic level by dynamic light scattering under oscillatory shear. By means of a two-time intensity correlation function (cf. Sec. III), dynamic light scattering allows one to quantify the evolution of the sample microscopic configuration during deformation. Representative experimental results are shown in fig. 10b, where the microscopic configuration of the sample at rest is compared with that of the sample under an oscillatory shear of amplitude $\gamma_0 = 0.4\%$ (fig. 10a).

Data for two wavevectors with equal magnitude $q = 3.1 \mu\text{m}^{-1}$ but different orientations, either parallel (\vec{q}_{\parallel}) or perpendicular (\vec{q}_{\perp}) to the shear direction, are compared. Both show a sudden drop as soon as the sample is deformed. This implies that the particles' relative position changes as a consequence of shear.

We emphasize the fact that a significant decorrelation is also observed along \vec{q}_{\perp} , indicating that the sample deformation is not purely affine. Nonaffine deformations can be interpreted in two different ways. They could be due to plastic, irreversible rearrangements Falk and Langer (1998) or they may originate from spatial fluctuations of the sample elastic modulus Basu *et al.* (2011); DiDonna and Lubensky (2005); Léonforte *et al.* (2006). Remarkably, we observe that for both components \vec{q}_{\parallel} and \vec{q}_{\perp} the correlation function increases again as the macroscopic deformation is reverted, and reaches values close to 1 when $\gamma(t) = 0$, e.g. for a time delay $\tau = 1/f$, f being the frequency of the oscillation: this behavior is referred to as *correlation echo* and has been reported for a variety of soft systems under an oscillatory deformation of modest amplitude Hébraud *et al.* (1997); Petekidis *et al.* (2002); Laurati *et al.* (2014); Rogers *et al.* (2014). The value of the correlation echo is very close to one, indicating that as the macroscopic deformation is recovered, the microscopic configuration reverts to that of the sample at rest. This unambiguously demonstrates that no plastic events occur during the oscillatory shear in the linear regime (cf. fig. 10c). In this regime, therefore, the non-affinities are due to spatial inhomogeneities of the sample elastic modulus, as reported for other network-forming systems Basu *et al.* (2011). Interestingly we note that non-affine reversible rearrangements have also been observed in the simulations of a gel in the linear regime and interpreted as a consequence of the extended floppy modes of the gel structure Colombo *et al.* (2013); Colombo and Del Gado (2014). The scenario depicted in the linear regime changes as soon as γ_0 is increased beyond the linear regime: as shown in fig. 10d, a sharp drop in the first correlation echo indicates the onset of irreversible rearrangements taking place in the nonlinear regime. This non-linear, irreversible regime is beyond the scope of this work. We simply mention that we have uncovered intriguing dynamical precursors of failure in the non-linear regime of creep tests Aime *et al.* (2018).

V. DISCUSSION AND CONCLUSION

We have investigated in detail the linear viscoelasticity of a fractal colloidal gel. Thanks to a combination of several rheological tests, we have demonstrated that the linear viscoelasticity can be very well described by a Fractional Maxwell model. This model depends on three parameters, an elastic modulus, a characteristic time and an exponent, α , which remain yet to be related to some underlying physical processes. We note that a fractional Kelvin-Voigt (FKV) model cannot account for our experimental data, since it predicts an increase of G'' with the frequency which is at odds with our measurements. Equivalently, one would not get an instantaneous elastic strain jump in creep with any Kelvin-Voigt-based model. Bouzid *et al.* (2018)

As mentioned in the introduction, an expression linking fractal dimension and power law rheology can be borrowed from the work of Muthukumar (1989) on critical gels. In the limit of screened hydrodynamic and excluded volume interactions, α is related to the fractal dimension d_f through $\alpha = [3(5 - 2d_f)]/[2(5 - d_f)]$. Using this expression, we find that the slight decrease of the exponent α of the FM model with sample age, from 0.45 to 0.35 (Fig. 5) would correspond to a fractal dimension slightly increasing from $d_f = 2.05$ to 2.15. Within the experimental error, this prediction is in excellent agreement with the value of d_f extracted from our scattering data (Fig. 2). Although we could not experimentally check the evolution of the fractal dimension with sample age as it requires a neutron beam, we note that a slow increase of d_f with sample age has previously been measured in more dilute colloidal gels Cipelletti *et al.* (2000). The quantitative agreement with Muthukumar's prediction, further strengthens the connection between the fractal structure and the power law rheology, extending it beyond the framework of critical gels discussed in Ref. Muthukumar (1989). This is actually intriguing, since the original derivation Muthukumar (1989)

was based on the assumption that the structure was scale-free, whereas in our case the fractal cluster size ξ clearly emerges from Fig. 2 as a characteristic length scale of the system. We note in addition that powerlaw rheology with a similar exponent 0.5 could also be observed in numerical works for gels for which the exponent could not be straightforwardly related to a fractal structure. Zia *et al.* (2014); Landrum *et al.* (2016); Bouzid *et al.* (2018) Moreover possible differences between the static microstructure and the structure of the stress-bearing backbone might be an issue.

The presence of a cluster network of well defined connectivity challenges the validity of the FM model at the smallest frequencies. The power law distribution of relaxation times assumed by the model implies for instance that the creep deformation reaches arbitrarily large values at times long enough, whereas one should expect a saturation to a terminal plateau deformation at long times somewhere beyond τ_{FM} . Unfortunately, such timescales are experimentally inaccessible, since the characteristic time grows linearly with sample age: as a consequence, any experiment probing a timescale beyond τ_{FM} would automatically be affected by aging. For this reason, the only way to test the consistency of FM at very small frequencies would be to repeat this analysis on different samples, for example changing the volume fraction. Based on a simple analysis with the time-cure superposition for polymer gels (see e.g. Adolf and Martin (1990)) and discussed in the introduction, one might expect that, with increasing volume fraction, the sample would be increasingly far away from the critical gel point: the range of length scales displaying self-similarity would be thus reduced and consequently one might expect an eventual terminal plateau to be shifted at higher frequencies.

On the other hand, we argue that the impossibility of addressing the putative loss peak around τ_{FM} in any clean experiment questions its physical relevance. The usual interpretation of a fractional rheological model is based on the existence of a power law distribution of relaxation times, of which τ_{FM} should represent some average value. However, one could argue about what physical interpretation should be attributed to relaxation times beyond the characteristic time for physical aging. Indeed, physical aging represents a true challenge for the fractional calculus-based framework presented in this paper, since it has to be introduced ‘by hand’ in the model in order to account for the experimental data. Therefore, one may wonder whether a more natural framework could exist that accounts for both the power law rheology and its time dependence. One potential candidate is Soft Glassy Rheology (SGR) Sollich *et al.* (1997), which considers that the sample mechanics is controlled by disorder, metastability and local structural rearrangements. The advantage of SGR is that aging emerges as a natural consequence of these features, and SGR predicts a virtual structural relaxation time linearly increasing with sample age Fielding *et al.* (2000), compatible with our findings. Within this framework, our gel would be represented by an effective ‘noise temperature’ $x = 1 - \alpha \sim 0.6$, well below the glass transition (which in SGR occurs at $x = 1$). The frequency spectrum of the sample is then predicted to be characterized by a nearly constant elastic modulus G' and a loss modulus $G'' \sim \omega^{x-1}$ Sollich (1998), which is in good agreement with the data in the experimentally accessible frequency range (Fig. 7). However, one feature that appears to be in stark contrast with the picture offered by SGR is the complete reversibility of the deformation, as demonstrated by the creep recovery experiments (see e.g. Fig. 8) and by the dynamic light scattering coupled to shear (Fig. 10). By contrast, in SGR creep is never completely recoverable, and the non-recoverable amount depends on the creep duration. Moreover, SGR predicts a logarithmic creep in the glassy regime ($x < 1$) Fielding *et al.* (2000), which is clearly incompatible with our experimental data (Fig. 4).

On the one hand, these considerations explicitly demonstrate that a thorough comparison between different rheological experiments allows one to discriminate between models that would be indistinguishable only looking at one kind of test, say oscillatory rheology. On the other hand, they raise the question of whether some concepts of SGR could be borrowed to provide a more natural framework to introduce aging in fractional models. This possibility opens intriguing perspectives for future theoretical works, aiming at a deeper understanding of the microscopic origin of power law rheology.

In addition, we have shown that non-affine but reversible rearrangements occur in the linear regime, thus hinting at a possible connection between reversible non-affinities and power law rheology. Relating those non affinities to some physical parameters as done in Basu *et al.* (2011) is delicate and would certainly deserve deeper investigation, by performing for instance spatially resolved measurements.

ACKNOWLEDGMENTS

This work was supported by the EU (Marie Skłodowska-Curie ITN Supolen, Grant No. 607937) and ANR (Grant No. ANR-14-CE32-0005-01). We are grateful to LLB for beam time and to Dafne Musino and Justine Pincemaille for the neutron scattering measurements. We also thank Thibaut Divoux for fruitful discussions.

REFERENCES

- B. Fabry, G. N. Maksym, J. P. Butler, M. Glogauer, D. Navajas, and J. J. Fredberg, “Scaling the Microrheology of Living Cells,” *Physical Review Letters* **87**, 148102 (2001).
- V. D. Djordjevic, J. Jaric, B. Fabry, J. J. Fredberg, and D. Stamenovic, “Fractional Derivatives Embody Essential Features of Cell Rheological Behavior,” *Annals of Biomedical Engineering* **31**, 692–699 (2003).
- N. Desprat, A. Richert, J. Simeon, and A. Asnacios, “Creep Function of a Single Living Cell,” *Biophysical Journal* **88**, 2224–2233 (2005).
- M. Balland, N. Desprat, D. Icard, S. Feriol, A. Asnacios, J. Browaeys, S. Hanon, and F. Gallet, “Power laws in microrheology experiments on living cells: Comparative analysis and modeling,” *Physical Review E* **74**, 021911 (2006).
- P. Kollmannsberger and B. Fabry, “Linear and Nonlinear Rheology of Living Cells,” *Annual Review of Materials Research* **41**, 75–97 (2011).
- F. M. Hecht, J. Rheinlaender, N. Schierbaum, W. H. Goldmann, B. Fabry, and T. E. Schoffer, “Imaging viscoelastic properties of live cells by AFM: Power-law rheology on the nanoscale,” *Soft Matter* **11**, 4584–4591 (2015).
- M. Kohandel, S. Sivaloganathan, G. Tenti, and K. Darvish, “Frequency dependence of complex moduli of brain tissue using a fractional Zener model,” *Physics in Medicine and Biology* **50**, 2799–2805 (2005).
- G. B. Davis, M. Kohandel, S. Sivaloganathan, and G. Tenti, “The constitutive properties of the brain parenchyma,” *Medical Engineering & Physics* **28**, 455–459 (2006).
- J. J. Shen, C. G. Li, H. T. Wu, and M. Kalantari, “Fractional order viscoelasticity in characterization for atrial tissue,” *Korea-Australia Rheology Journal* **25**, 87–93 (2013).
- F. Gobeaux, E. Belamie, G. Mosser, P. Davidson, and S. Asnacios, “Power law rheology and strain-induced yielding in acidic solutions of type I-collagen,” *Soft Matter* **6**, 3769 (2010).
- D. J. Curtis, A. Holder, N. Badiei, J. Claypole, M. Walters, B. Thomas, M. Barrow, D. Deganello, M. R. Brown, P. R. Williams, and K. Hawkins, “Validation of Optimal Fourier Rheometry for rapidly gelling materials and its application in the study of collagen gelation,” *Journal of Non-Newtonian Fluid Mechanics* **222**, 253–259 (2015).
- B. Józwiak, M. Orczykowska, and M. Dziubiński, “Fractional generalizations of maxwell and Kelvin-Voigt models for biopolymer characterization,” *PloS one* **10**, e0143090 (2015).
- L. Ma and G. V. Barbosa-Cánovas, “Simulating viscoelastic properties of selected food gums and gum mixtures using a fractional derivative model,” *Journal of texture studies* **27**, 307–325 (1996).
- N. Zhou and S. J. Mulvaney, “The effect of milk fat, the ratio of casein to water, and temperature on the viscoelastic properties of rennet casein gels,” *Journal of Dairy Science* **81**, 2561–2571 (1998).
- R. Subramanian, K. Muthukumarappan, and S. Gunasekaran, “Linear Viscoelastic Properties of Regular- and Reduced-Fat Pasteurized Process Cheese During Heating and Cooling,” *International Journal of Food Properties* **9**, 377–393 (2006).
- T. S. K. Ng and G. H. McKinley, “Power law gels at finite strains: The nonlinear rheology of gluten gels,” *Journal of Rheology* **52**, 417–449 (2008).
- M. Caggioni, P. T. Spicer, D. L. Blair, S. E. Lindberg, and D. A. Weitz, “Rheology and microrheology of a microstructured fluid: The gellan gum case,” *Journal of Rheology* **51**, 851–865 (2007).
- J. Korus, M. Witzczak, R. Ziobro, and L. Juszczak, “The impact of resistant starch on characteristics of gluten-free dough and bread,” *Food Hydrocolloids* **23**, 988–995 (2009).
- R. Moreira, F. Chenlo, and M. D. Torres, “Rheology of commercial chestnut flour doughs incorporated with gelling agents,” *Food Hydrocolloids* **25**, 1361–1371 (2011).
- F. Ronda, S. Perez-Quirce, A. Angioloni, and C. Collar, “Impact of viscous dietary fibres on the viscoelastic behaviour of gluten-free formulated rice doughs: A fundamental and empirical rheological approach,” *Food Hydrocolloids* **32**, 252–262 (2013).

- Z. Xu and W. Chen, "A fractional-order model on new experiments of linear viscoelastic creep of Hami Melon," *Computers & Mathematics with Applications* **66**, 677–681 (2013).
- A. Jaishankar and G. H. McKinley, "A fractional K-BKZ constitutive formulation for describing the non-linear rheology of multiscale complex fluids," in *Journal of Rheology (1978-present)*, Vol. 58 (2014) pp. 1751–1788.
- M. Leocmach, C. Perge, T. Divoux, and S. Manneville, "Creep and Fracture of a Protein Gel under Stress," *Physical Review Letters* **113**, 038303 (2014).
- T. J. Faber, A. Jaishankar, and G. H. McKinley, "Describing the firmness, springiness and rubberiness of food gels using fractional calculus. Part I: Theoretical framework," *Food Hydrocolloids* **62**, 311–324 (2017a).
- T. J. Faber, A. Jaishankar, and G. H. McKinley, "Describing the firmness, springiness and rubberiness of food gels using fractional calculus. Part II: Measurements on semi-hard cheese," *Food Hydrocolloids* **62**, 325–339 (2017b).
- J. P. Rich, G. H. McKinley, and P. S. Doyle, "Size dependence of microprobe dynamics during gelation of a discotic colloidal clay," *Journal of Rheology* **55**, 273–299 (2011).
- P. Lidon, L. Villa, and S. Manneville, "Power-law creep and residual stresses in a carboxypol gel," *Rheologica Acta* **56**, 307–323 (2017).
- K.-C. Hung, U.-S. Jeng, and S.-H. Hsu, "Fractal Structure of Hydrogels Modulates Stem Cell Behavior," *ACS Macro Letters* **4**, 1056–1061 (2015).
- F. Chambon, Z. S. Petrovic, W. J. MacKnight, and H. H. Winter, "Rheology of model polyurethanes at the gel point," *Macromolecules* **19**, 2146–2149 (1986).
- H. H. Winter and F. Chambon, "Analysis of Linear Viscoelasticity of a Crosslinking Polymer at the Gel Point," *Journal of Rheology* **30**, 367–382 (1986).
- D. Durand, M. Delsanti, M. Adam, and J. M. Luck, "Frequency dependence of viscoelastic properties of branched polymers near gelation threshold," *EPL (Europhysics Letters)* **3**, 297 (1987).
- J. E. Martin, D. Adolf, and J. P. Wilcoxon, "Viscoelasticity of near-critical gels," *Physical review letters* **61**, 2620 (1988).
- D. Adolf and J. E. Martin, "Time-cure superposition during crosslinking," *Macromolecules* **23**, 3700–3704 (1990).
- V. Tirtaatmadja, K. C. Tam, and R. D. Jenkins, "Superposition of oscillations on steady shear flow as a technique for investigating the structure of associative polymers," *Macromolecules* **30**, 1426–1433 (1997).
- T. H. Larsen and E. M. Furst, "Micro-rheology of the Liquid-Solid Transition during Gelation," *Physical Review Letters* **100**, 146001 (2008).
- L. Leibler, M. Rubinstein, and R. H. Colby, "Dynamics of reversible networks," *Macromolecules* **24**, 4701–4707 (1991).
- D. J. Plazek, "Dynamic mechanical and creep properties of a 23% cellulose nitrate solution; Andrade creep in polymeric systems," *Journal of Colloid Science* **15**, 50–75 (1960).
- A. Hernández-Jiménez, J. Hernández-Santiago, A. Macías-García, and J. Sánchez-González, "Relaxation modulus in PMMA and PTFE fitting by fractional Maxwell model," *Polymer Testing* **21**, 325–331 (2002).
- C. Friedrich, H. Schiessel, and A. Blumen, "Constitutive behavior modeling and fractional derivatives," *Rheology Series Advances in the Flow and Rheology of Non-Newtonian Fluids*, **8**, 429–466 (1999).
- J. G. Curro and P. Pincus, "A theoretical basis for viscoelastic relaxation of elastomers in the long-time limit," *Macromolecules* **16**, 559–562 (1983).
- H. H. Winter and M. Mours, "Rheology of polymers near liquid-solid transitions," in *Advances in Polymer Science* (B. Ewen, 1999).
- J. D. Ferry, *Viscoelastic Properties of Polymers* (John Wiley and Sons, 1980).
- R. Metzler, W. Schick, H. Kilian, and T. F. Nonnenmacher, "Relaxation in filled polymers: A fractional calculus approach," *The Journal of Chemical Physics* **103**, 7180–7186 (1995).
- P. Sollich, F. Lequeux, P. Hébraud, and M. E. Cates, "Rheology of soft glassy materials," *Physical review letters* **78**, 2020 (1997).
- P. Sollich, "Rheological constitutive equation for a model of soft glassy materials," *Physical Review E* **58**, 738 (1998).
- R. H. Colby and M. Rubinstein, *Polymer Physics* (Oxford University Press, 2003).
- D. Stauffer and A. Aharony, *Introduction to Percolation Theory, 2nd Revised Edition* (Taylor & Francis, 2003).
- J. E. Martin and D. Adolf, "The sol-gel transition in chemical gels," *Annual review of physical chemistry* **42**, 311–339 (1991).
- M. Muthukumar, "Screening effect on viscoelasticity near the gel point," *Macromolecules* **22**, 4656–4658 (1989).
- P. Patrício, C. R. Leal, J. Duarte, and C. Januário, "Rheology of the cytoskeleton as a fractal network," *Physical Review E* **92**, 040702 (2015).
- M. Dahesh, A. Banc, A. Duri, M.-H. Morel, and L. Ramos, "Spontaneous gelation of wheat gluten proteins in a food grade solvent," *Food Hydrocolloids* **52**, 1–10 (2016).
- M. Takenaka, T. Kobayashi, K. Saijo, H. Tanaka, N. Iwase, T. Hashimoto, and M. Takahashi, "Comparison in fractal dimension between those obtained from structure factor and viscoelasticity of gel networks of 1,3:2,4-bis-O-(p-methylbenzylidene)-D-sorbitol in polystyrene melt at gel point," *The Journal of Chemical Physics* **121**, 3323–3328 (2004).

- T. Matsumoto, M. Kawai, and T. Masuda, “Viscoelastic and SAXS investigation of fractal structure near the gel point in alginate aqueous systems,” *Macromolecules* **25**, 5430–5433 (1992).
- M. Helmberger, M. Pienn, M. Urschler, P. Kullnig, R. Stollberger, G. Kovacs, A. Olschewski, H. Olschewski, and Z. Bálint, “Quantification of Tortuosity and Fractal Dimension of the Lung Vessels in Pulmonary Hypertension Patients,” *PLoS ONE* **9**, e87515 (2014).
- B. Mauroy, M. Filoche, E. R. Weibel, and B. Sapoval, “An optimal bronchial tree may be dangerous,” *Nature* **427**, 633–636 (2004).
- K. Ahmadi, M. Ahmadlou, M. Rezazade, E. Azad-Marzabadi, and F. Sajedi, “Brain activity of women is more fractal than men,” *Neuroscience Letters* **535**, 7–11 (2013).
- M. Carpineti and M. Giglio, “Transition from semiorde to disorder in the aggregation of dense colloidal solutions,” *Physical Review Letters* **70**, 3828 (1993).
- L. G. B. Bremer, B. H. Bijsterbosch, R. Schrijvers, T. Van Vliet, and P. Walstra, “On the fractal nature of the structure of acid casein gels,” *Colloids and Surfaces* **51**, 159–170 (1990).
- P. Duval, M. Montagnat, F. Grennerat, J. Weiss, J. Meyssonier, and A. Philip, “Creep and plasticity of glacier ice: A material science perspective,” *Journal of Glaciology* **56**, 1059–1068 (2010).
- J. Paredes, M. A. J. Michels, and D. Bonn, “Rheology across the Zero-Temperature Jamming Transition,” *Physical Review Letters* **111**, 015701 (2013).
- E. N. Andrade, “On the Viscous Flow in Metals, and Allied Phenomena,” *Proceedings of the Royal Society A: Mathematical and Physical Sciences* **84**, 1–12 (1910).
- M.-C. Miguel, A. Vespignani, M. Zaiser, and S. Zapperi, “Dislocation Jamming and Andrade Creep,” *Physical Review Letters* **89**, 165501 (2002).
- J.-P. Poirier, *Creep of Crystals* (Cambridge University Press, 1985).
- A. H. Cottrell, “The time laws of creep,” *Journal of the Mechanics and Physics of Solids* **1**, 53–63 (1952).
- M. F. Ashby and P. Duval, “The creep of polycrystalline ice,” *Cold Regions Science and Technology* **11**, 285–300 (1985).
- M. Siebenbürger, M. Ballauff, and T. Voigtmann, “Creep in Colloidal Glasses,” *Physical Review Letters* **108**, 255701 (2012).
- T. Sentjabrskaja, P. Chaudhuri, M. Hermes, W. C. K. Poon, J. Horbach, S. U. Egelhaaf, and M. Laurati, “Creep and flow of glasses: Strain response linked to the spatial distribution of dynamical heterogeneities,” *Scientific Reports* **5**, 11884 (2015).
- P. Coussot, H. Tabuteau, X. Chateau, L. Tocquer, and G. Ovarlez, “Aging and solid or liquid behavior in pastes,” *Journal of Rheology* **50**, 975 (2006).
- F. Caton and C. Baravian, “Plastic behavior of some yield stress fluids: From creep to long-time yield,” *Rheologica Acta* **47**, 601–607 (2008).
- H. Nechad, A. Helmstetter, R. El Guerjouma, and D. Sornette, “Creep Ruptures in Heterogeneous Materials,” *Physical Review Letters* **94**, 045501 (2005).
- S. N. Karobi, T. L. Sun, T. Kurokawa, F. Luo, T. Nakajima, T. Nonoyama, and J. P. Gong, “Creep Behavior and Delayed Fracture of Tough Polyampholyte Hydrogels by Tensile Test,” *Macromolecules* **49**, 5630–5636 (2016).
- E. Ghiringhelli, D. Roux, D. Bleses, H. Galliard, and F. Caton, “Optimal fourier rheometry: Application to the gelation of an alginate,” *Rheologica Acta* **51**, 413–420 (2012).
- M. Bouzid, B. Keshavarz, M. Geri, T. Divoux, E. Del Gado, and G. H. McKinley, “Computing the linear viscoelastic properties of soft gels using an optimally windowed chirp protocol,” *Journal of Rheology* **62**, 1037–1050 (2018).
- M. Geri, B. Keshavarz, T. Divoux, C. Clasen, D. J. Curtis, and G. H. McKinley, “Time-Resolved Mechanical Spectroscopy of Soft Materials via Optimally Windowed Chirps,” arXiv:1804.03061 (2018).
- J. M. Cherièr, L. Belec, and J. L. Gacougnolle, “The three successive stages of creep of PMMA between 55 C and 90 C,” *Polymer Engineering & Science* **37**, 1664–1671 (1997).
- M. Carpineti, M. Giglio, and V. Degiorgio, “Mass conservation and anticorrelation effects in the colloidal aggregation of dense solutions,” *Physical Review E* **51**, 590 (1995).
- L. Cipelletti, S. Manley, R. C. Ball, and D. A. Weitz, “Universal aging features in the restructuring of fractal colloidal gels,” *Physical review letters* **84**, 2275 (2000).
- R. Hilfer, *Applications of fractional calculus in physics* (World Scientific, 2000).
- A. Jaishankar and G. H. McKinley, “Power-law rheology in the bulk and at the interface: quasi-properties and fractional constitutive equations,” in *Proceedings of the Royal Society of London A: Mathematical, Physical and Engineering Sciences*, Vol. 469 (The Royal Society, 2013) p. 20120284.
- E. Demirci and N. Ozalp, “A method for solving differential equations of fractional order,” *Journal of Computational and Applied Mathematics* **236**, 2754–2762 (2012).
- G. W. S. Blair, D. Sc, B. C. Veinoglou, Ph D, J. E. Caffyn, and B. Sc, “Limitations of the Newtonian time scale in relation to non-equilibrium rheological states and a theory of quasi-properties,” *Proc. R. Soc. Lond. A* **189**, 69–87 (1947).
- R. L. Bagley and P. J. Torvik, “A Theoretical Basis for the Application of Fractional Calculus to Viscoelasticity,” *Journal of Rheology* **27**, 201–210 (1983).
- R. L. Bagley and P. J. Torvik, “On the Fractional Calculus Model of Viscoelastic Behavior,” *Journal of Rheology* **30**, 133–155 (1986).
- R. L. Bagley, “Power law and fractional calculus model of viscoelasticity,” *AIAA Journal* **27**, 1412–1417 (1989).

- H. M. Wyss, J. Innerlohinger, L. P. Meier, L. J. Gauckler, and O. Glatter, “Small-angle static light scattering of concentrated silica suspensions during in situ destabilization,” *Journal of Colloid and Interface Science* **271**, 388–399 (2004).
- E. Tamborini and L. Cipelletti, “Multiangle static and dynamic light scattering in the intermediate scattering angle range,” *Review of Scientific Instruments* **83**, 093106 (2012).
- S. Aime, L. Ramos, J. M. Fromental, G. Prevot, R. Jelinek, and L. Cipelletti, “A stress-controlled shear cell for small-angle light scattering and microscopy,” *Review of Scientific Instruments* **87**, 123907 (2016).
- S. Aime, L. Ramos, and L. Cipelletti, “Microscopic dynamics and failure precursors of a gel under mechanical load,” *Proc Natl Acad Sci USA* **115**, 3587–3592 (2018).
- T. Zemb and P. Lindner, eds., *Neutron, X-Rays and Light. Scattering Methods Applied to Soft Condensed Matter*, 1st ed. (North Holland, Amsterdam ; Boston, 2002).
- B. J. Berne and R. Pecora, *Dynamic Light Scattering: With Applications to Chemistry, Biology, and Physics* (Courier Corporation, 2013).
- I. Bressler, J. Kohlbrecher, and A. F. Thunemann, “SASfit: a tool for small-angle scattering data analysis using a library of analytical expressions,” *Journal of Applied Crystallography* **48**, 1587–1598 (2015).
- S. Manley, J. M. Skotheim, L. Mahadevan, and D. A. Weitz, “Gravitational Collapse of Colloidal Gels,” *Physical Review Letters* **94**, 218302 (2005a).
- M. Carpinetti and M. Giglio, “Spinodal-type dynamics in fractal aggregation of colloidal clusters,” *Physical Review Letters* **68**, 3327–3330 (1992).
- L. Cipelletti and L. Ramos, “Slow dynamics in glassy soft matter,” *Journal of Physics: Condensed Matter* **17**, R253–R285 (2005).
- S. Manley, B. Davidovitch, N. R. Davies, L. Cipelletti, A. E. Bailey, R. J. Christianson, U. Gasser, V. Prasad, P. N. Segre, M. P. Doherty, S. Sankaran, A. L. Jankovsky, B. Shiley, J. Bowen, J. Eggers, C. Kurta, T. Lorik, and D. A. Weitz, “Time-Dependent Strength of Colloidal Gels,” *Physical Review Letters* **95**, 048302 (2005b).
- N. Koumakis and G. Petekidis, “Two step yielding in attractive colloids: Transition from gels to attractive glasses,” *Soft Matter* **7**, 2456 (2011).
- H. Guo, S. Ramakrishnan, J. L. Harden, and R. L. Leheny, “Gel formation and aging in weakly attractive nanocolloid suspensions at intermediate concentrations,” *The Journal of Chemical Physics* **135**, 154903 (2011).
- D. C. E. Calzolari, I. Bischofberger, F. Nazzari, and V. Trappe, “Interplay of coarsening, aging, and stress hardening impacting the creep behavior of a colloidal gel,” *Journal of Rheology* **61**, 817–831 (2017).
- R. M. L. Evans, M. Tassieri, D. Auhl, and T. A. Waigh, “Direct conversion of rheological compliance measurements into storage and loss moduli,” *Physical Review E* **80**, 012501 (2009).
- J. D. Park, K. H. Ahn, and N. J. Wagner, “Structure-rheology relationship for a homogeneous colloidal gel under shear startup,” *Journal of Rheology* **61**, 117–137 (2017).
- J. Colombo and E. Del Gado, “Stress localization, stiffening, and yielding in a model colloidal gel,” *Journal of Rheology* **58**, 1089–1116 (2014).
- M. Bouzid and E. Del Gado, “Network Topology in Soft Gels: Hardening and Softening Materials,” *Langmuir* **34**, 773–781 (2018).
- S. Jamali, G. H. McKinley, and R. C. Armstrong, “Microstructural Rearrangements and their Rheological Implications in a Model Thixotropic Elastoviscoplastic Fluid,” *Physical Review Letters* **118**, 048003 (2017).
- A. Mohraz and M. J. Solomon, “Orientation and rupture of fractal colloidal gels during start-up of steady shear flow,” *Journal of Rheology* **49**, 657 (2005).
- J. Vermant and M. J. Solomon, “Flow-induced structure in colloidal suspensions,” *Journal of Physics: Condensed Matter* **17**, R187 (2005).
- J. M. Kim, A. P. Eberle, A. K. Gurnon, L. Porcar, and N. J. Wagner, “The microstructure and rheology of a model, thixotropic nanoparticle gel under steady shear and large amplitude oscillatory shear (LAOS),” *Journal of Rheology (1978-present)* **58**, 1301–1328 (2014).
- M. L. Falk and J. S. Langer, “Dynamics of viscoplastic deformation in amorphous solids,” *Physical Review E* **57**, 7192 (1998).
- A. Basu, Q. Wen, X. Mao, T. C. Lubensky, P. A. Janmey, and A. G. Yodh, “Nonaffine displacements in flexible polymer networks,” *Macromolecules* **44**, 1671–1679 (2011).
- B. A. DiDonna and T. C. Lubensky, “Nonaffine correlations in random elastic media,” *Physical Review E* **72**, 066619 (2005).
- F. Léonforte, A. Tanguy, J. P. Wittmer, and J.-L. Barrat, “Inhomogeneous Elastic Response of Silica Glass,” *Physical Review Letters* **97**, 055501 (2006).
- P. Hébraud, F. Lequeux, J. P. Munch, and D. J. Pine, “Yielding and rearrangements in disordered emulsions,” *Physical Review Letters* **78**, 4657 (1997).
- G. Petekidis, A. Moussaïd, and P. N. Pusey, “Rearrangements in hard-sphere glasses under oscillatory shear strain,” *Physical Review E* **66**, 051402 (2002).
- M. Laurati, S. U. Egelhaaf, and G. Petekidis, “Plastic rearrangements in colloidal gels investigated by LAOS and LS-Echo,” *Journal of Rheology* **58**, 1395–1417 (2014).
- M. C. Rogers, K. Chen, L. Andrzejewski, S. Narayanan, S. Ramakrishnan, R. L. Leheny, and J. L. Harden, “Echoes in x-ray speckles track nanometer-scale plastic events in colloidal gels under shear,” *Physical Review E* **90**, 062310 (2014).

- J. Colombo, A. Widmer-Cooper, and E. Del Gado, "Microscopic Picture of Cooperative Processes in Restructuring Gel Networks," *Physical Review Letters* **110**, 198301 (2013).
- R. N. Zia, B. J. Landrum, and W. B. Russel, "A micro-mechanical study of coarsening and rheology of colloidal gels: Cage building, cage hopping, and Smoluchowski's ratchet," *Journal of Rheology* (1978-present) **58**, 1121–1157 (2014).
- B. J. Landrum, W. B. Russel, and R. N. Zia, "Delayed yield in colloidal gels: Creep, flow, and re-entrant solid regimes," *Journal of Rheology* (1978-present) **60**, 783–807 (2016).
- S. M. Fielding, P. Sollich, and M. E. Cates, "Aging and rheology in soft materials," *Journal of Rheology* **44**, 323–369 (2000).

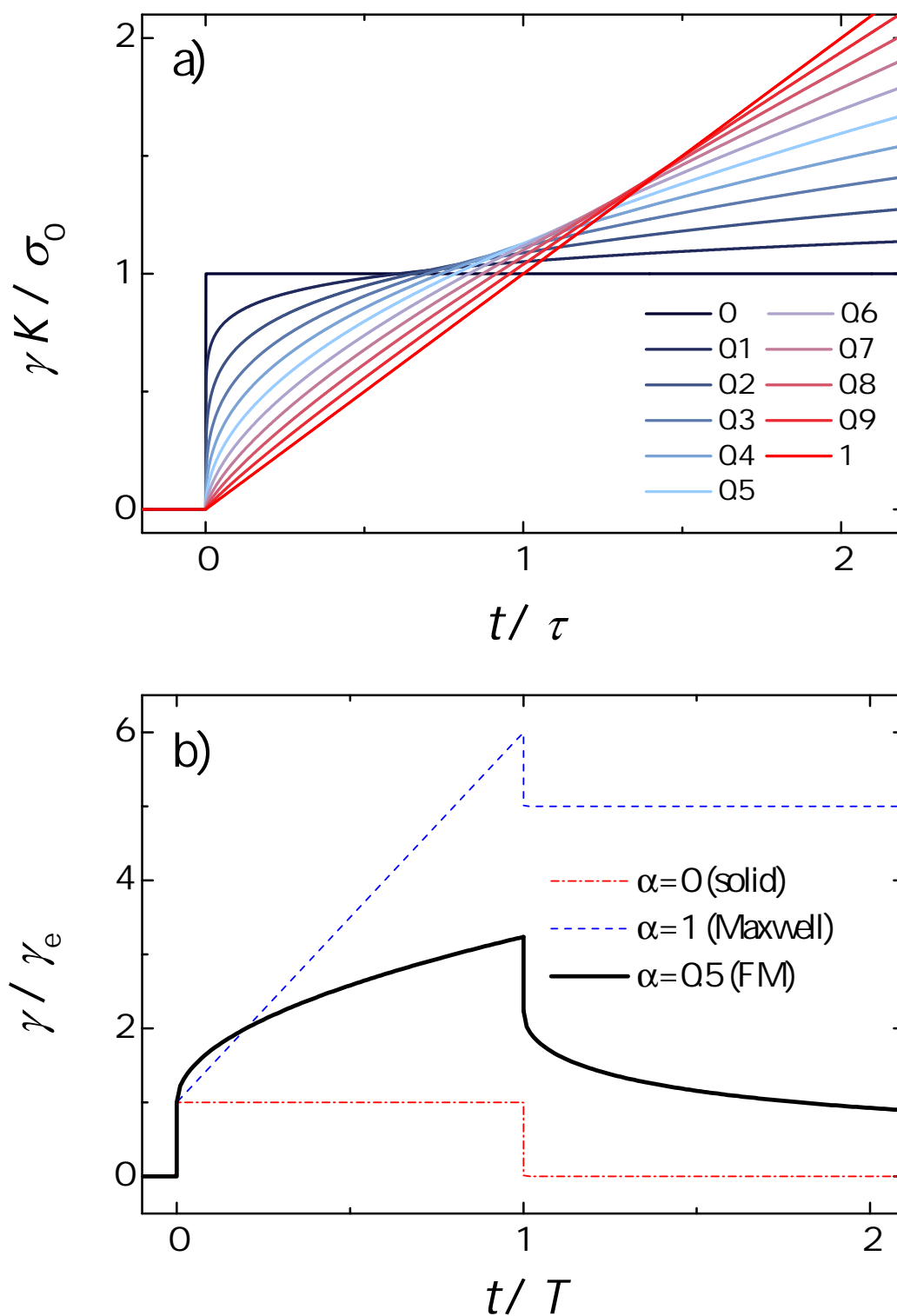


FIG. 1. a) Normalized strain as a function of the normalized time upon application of a constant stress of amplitude σ_0 applied at time 0 for a springpot with different exponents α as indicated in the legend. b) Time evolution of the strain normalized by the initial elastic jump during the creep and recovery of an elastic solid ($\alpha = 0$), a Maxwell fluid ($\alpha = 1$) and a fractional Maxwell fluid with an exponent $\alpha = 0.5$.

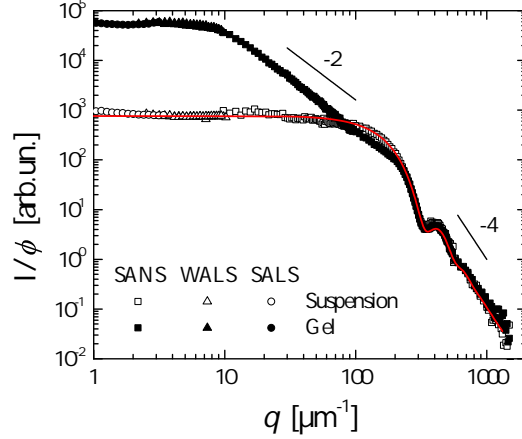


FIG. 2. Scattered intensity of the colloidal gel at $\phi = 5\%$ volume fraction (filled symbols) and of a stable colloidal suspension, at $\phi = 0.037\%$ (empty symbols), probed with small angle neutron scattering, wide-and X ray scattering and static light scattering, as indicated in the legend. Red line: fitted form factor of a polydisperse set of spheres of average diameter 25 nm and polydispersity 10%.

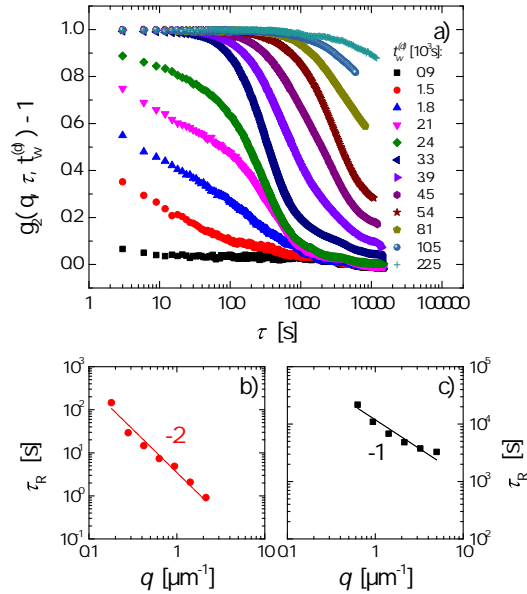


FIG. 3. (a) Intensity correlation functions plotted as a function of time delay, τ , for different times $t_w^{(d)}$ after the onset of aggregation. The scattering vector is $q = 1.5 \mu\text{m}^{-1}$. (b,c) Relaxation times extracted from correlation functions during the aggregation stages ($t_w^{(d)} = 1200$ s, red circles) and once a network is formed ($t_w^{(d)} = 5000$ s, black squares), and plotted as a function of q . The lines are power law fits with exponent -2 (aggregation stage) (b) and -1 (gel stage) (c).

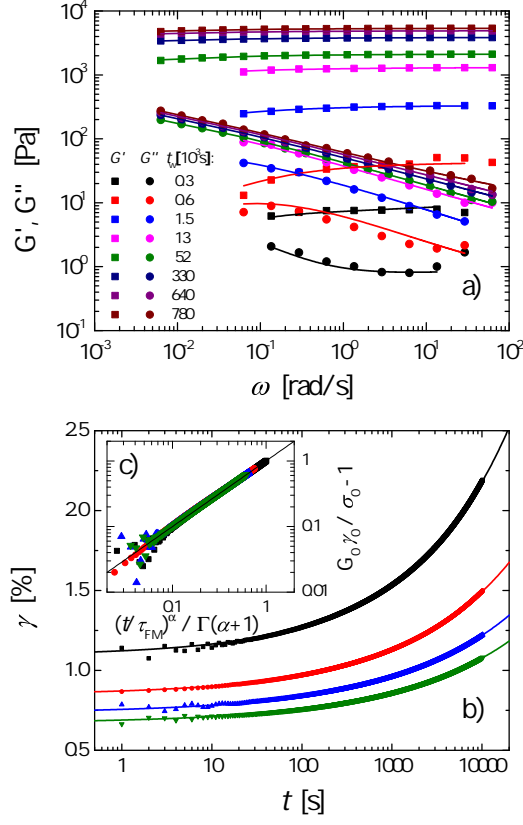


FIG. 4. (a) Viscoelastic moduli measured during sample aging at a strain amplitude $\gamma_0 = 0.1\%$, and plotted as a function of angular frequency for different waiting times t_w as indicated in the legend. Solid lines represent fits using Eqs. 5 and 6. The fit parameters (stars) are displayed in figure 5. (b) Creep deformation under a shear stress $\sigma_0 = 30$ Pa for 4 different sample ages, from top to bottom $t_w = 12 \times 10^4, 26 \times 10^4, 40 \times 10^4, 54 \times 10^4$ s. Lines are fits of the experimental data using Eq. 7. The fit parameters (filled squares) are shown in Fig. 5. (c) Same data as in (b) plotted in rescaled units (see text) (symbols) and theoretical expectation (line).

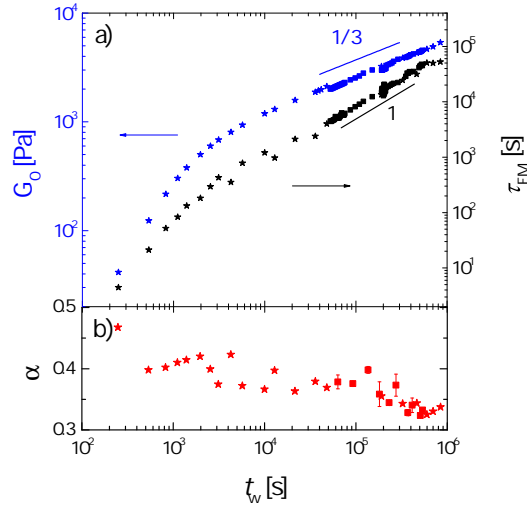


FIG. 5. Fractional Maxwell parameters extracted from both frequency sweeps (stars) and creep data (squares) fitted by Eqs. 5, 6 and 7 respectively.

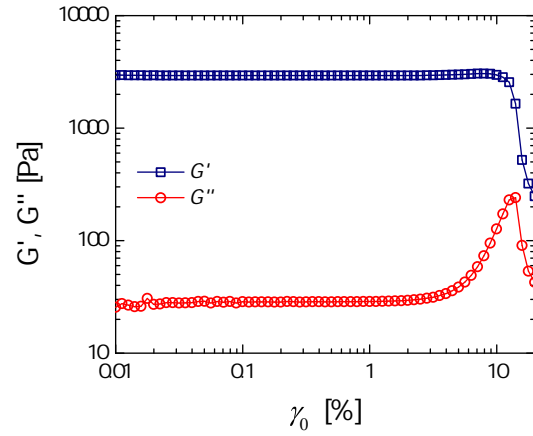


FIG. 6. Viscoelastic moduli G' (squares) and G'' (circles) probed at angular frequency $\omega = 6.28$ Hz as a function of the strain amplitude, γ_0 . γ_0 is increased from 0.01% to 1000% at a rate of 20 points per decade. 10 oscillations are performed for each γ_0 . Sample age is 240000 s.

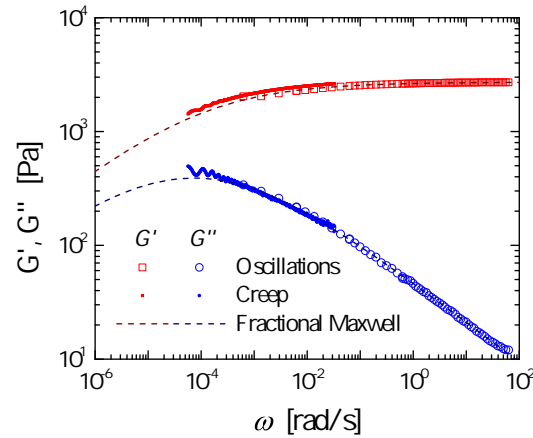


FIG. 7. Comparison between viscoelastic moduli probed in small amplitude oscillatory strain at $\gamma_0 = 0.1\%$ amplitude (large open symbols) and creep under a constant shear stress $\sigma_0/G_0 = 1.8\%$ (small solid points) for a sample age $t_w = 2 \cdot 10^5$ s. Dashed lines represent best fits using the Fractional Maxwell model. The fit parameters are: $G_0 = 2700$ Pa, $\tau_M = 1.5 \cdot 10^4$ s, $\alpha = 0.35$.

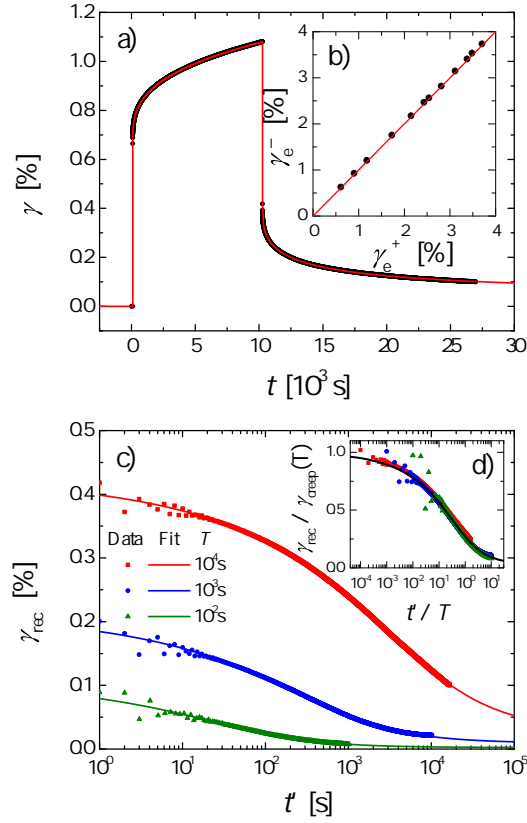


FIG. 8. (a) Viscoelastic creep under a constant shear stress $\sigma_0 = 30$ Pa, lasting a time $T = 10000$ s and followed by creep recovery. The symbols are experimental data and the line is a fit with the FM model yielding $G_0 = 4400$ Pa, $\tau_{FM} = 4.8 \cdot 10^4$ s, $\alpha = 0.33$. (b) Recovery downwards jump γ_e^- plotted as a function of the instantaneous upward elastic jump $\gamma_e^+ = \sigma_0/G_0$. Red line represents the expected $\gamma_e^+ = \gamma_e^-$ behavior. (c) Creep recovery curves following a creep under a stress $\sigma_0 = 30$ Pa lasting T seconds, as specified in the legend. The symbols are the experimental data points and the line is the best fit with FM model. (d) Same data plotted in rescaled units, $\gamma_{\text{rec}}/\gamma_{\text{creep}}$ as a function of the rescaled time t'/T , as in Eq. 9. The sample age is $t_w \approx 5 \cdot 10^5$ s.

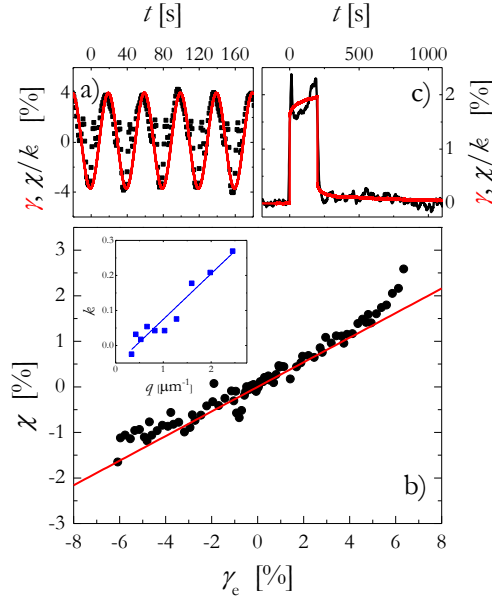


FIG. 9. a) Red symbols: oscillating strain under an oscillating stress of amplitude $\sigma_0/G_0 = 4\%$. Black line: static asymmetry $\chi(q)$ measured at $q = 2.6\mu\text{m}^{-1}$ divided by the proportionality constant $k(q)$ discussed in the text. b) Symbols: static asymmetry $\chi(q = 2.6\mu\text{m}^{-1})$ observed under a step strain deformation of amplitude γ_e . Positive and negative γ_e values represent step strains in opposite directions. Red line: linear fit of the small deformation regime, used to extract the proportionality constant $k(q)$. Inset: q dependence of the proportionality constant. The line is a linear fit of the experimental data (symbols). c) Red curve: creep deformation ($\sigma_0/G_0 = 1.5\%$) and recovery after a creep time $T = 200$ s. Black curve: static asymmetry $\chi(q = 2.6\mu\text{m}^{-1})$ divided by $k(q)$. Sample age is $t_w = 1.5 \times 10^5$ s.

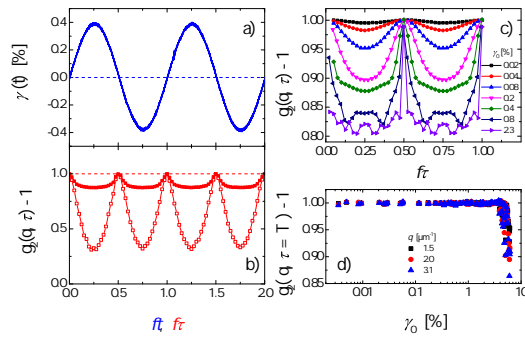


FIG. 10. a) Oscillating strain under an oscillating stress of amplitude $\sigma_0/G_0 = 0.4\%$ as a function of adimensional time ft ($f = 0.025$ Hz is the frequency of the oscillation). b) Intensity correlation function measured for q vectors oriented in the velocity direction (open symbols) and in the vorticity direction (filled symbols), respectively. Correlation echoes occur whenever the macroscopic deformation goes through 0. c) Correlation functions measured in the vorticity direction for various strain amplitudes γ_0 , as shown by the label. In b) and c) the scattering vector is $q = 3.1\mu\text{m}^{-1}$. d) Amplitude of the correlation echo as a function of the strain amplitude γ_0 , for three representative scattering vectors. Sample age is $t_w = 1.5 \times 10^5$ s.